Asia-Pac. J. Atmos. Sci., 51(3), 259-274, 2015
DOI:10.1007/s13143-015-0076-3
pISSN 1976-7633 / eISSN 1976-7951

Origin, Evolution and Structure of Meso-α-Scale Lows Associated with Cloud Clusters and Heavy Rainfall over the Korean Peninsula

Uju Shin and Tae-Young Lee

Department of Atmospheric Sciences and Global Environment Laboratory, Yonsei University, Seoul, Korea

(Manuscript received 25 February 2015; accepted 3 August 2015)
© The Korean Meteorological Society and Springer 2015

Abstract: An investigation was conducted to describe the locations of initial occurrence, evolution and structure of meso-α-scale lows (MLs) associated with cloud clusters and heavy rainfall over the Korean Peninsula using observation and reanalysis data. We selected 29 heavy rainfall events associated with MLs during the 10-year period of 2001-2010. The locations of initial ML occurrence are widely spread from the eastern flank of the Tibetan Plateau to the Yellow Sea. These locations are grouped into 3 regions: 1) the eastern flank of the Tibetan Plateau (R1, 6 cases), 2) central and eastern China (R2, 16 cases), and 3) the Yellow Sea (R3, 7 cases). Initial MLs tend to occur within a deep trough over the eastern flank of the Tibetan Plateau (R1 cases) or a long trough extended northeastward from the southeast of the Tibetan Plateau along the northwestern rim of the western Pacific subtropical high (a majority of R2 cases and two R3 cases). Horizontal temperature gradients are weak over the areas of initial MLs. Meso-α-scale lows tend to develop in the lower troposphere (e.g., below 700 hPa) in an environment of existing cyclonic vorticity. And they are accompanied by anticyclonic vorticity in the upper troposphere. The speed of ML movement varies with each case and with the location of ML. The average speeds of ML movement are 32.4, 37.2 and 40.4 km h^{-1} for the R1, R2 and R3 groups, respectively. Meso-α-scale lows are shown to have a warm-core structure in general. They are tilted toward various directions with a majority of them (14 of 29 MLs) tilting northward with height.

Key words: Meso-α-scale lows, cloud clusters, initial occurrence locations, heavy rainfall

1. Introduction

Meso-α-scale lows (MLs) associated with heavy rainfall events are frequently observed along the Baiu/Changma/Mei-yu fronts (e.g., Matsumoto et al., 1970; Ninomiya and Akiyama, 1971; Park et al., 1986; Ding et al., 2001; You et al., 2010; Zhang et al., 2014), and the relationship between such frontal depressions and heavy rainfall is the subject of considerable research. Based on several Japanese studies (e.g., Yoshizumi, 1977; Akiyama, 1978; Ninomiya and Yamazaki, 1979), Ninomiya and Muraki (1986) noted that intense Baiu precipitation was produced by the successive development of meso-α-scale frontal depressions. Various studies examined the relationships between Mei-yu frontal lows and heavy rainfall in the Yangtze River Basin (e.g., Bei et al., 2002; Qian et al., 2005; Zhang et al., 2014)

Several studies have been conducted to understand the formation and evolution of MLs along the Mei-yu and Baiu fronts. The eastern flank of the Tibetan Plateau is an important origin of MLs along these fronts (Akiyama, 1984; Murakami and Huang, 1984; Chen and DelliOsso 1986; Wang and Orlanski, 1987; Ding et al., 2001; Wang et al., 2004). Akiyama (1984) found that a cloud cluster was generated at the eastern foot of the Tibetan Plateau and propagated eastward with a phase speed of ~1000 km day^{-1} and was accompanied by a weak positive vorticity core in the mid-troposphere. Based on GMS infrared brightness temperature observations in May-August 1998-2001, Wang et al. (2004) also found that convective cloud streaks propagated eastward from the eastern edge of the Tibetan Plateau, and that the zonal span and duration of episodes could reach 3000 km and 45 h, respectively. Ding et al. (2001) identified a succession of MLs (vortices) along the Mei-yu frontal zones in 1998 and 1999, which mostly originated along the eastern flank of the Tibetan Plateau and migrated eastward, with vortex centers located to the north of the low-level jet axis and heavy rainfall southeast of the disturbances. Chen et al. (1991) noted a relatively frequent cyclogenesis southwest of the Shandong Peninsula during summer, although they excluded monsoon depressions.

Meso-α-scale lows experience changes in their environment as they move along the Mei-yu and Baiu fronts. Ninomiya and Akiyama (1992) suggested that the structure of Baiu fronts varied with longitude: a typical polar front with a deep baroclinic structure over the Baiu front at 135-160°E, a shallow structure (that is, the vorticity was confined to the lower layer) at 100-120°E, and a transition zone at 120-135°E. Akiyama (1984) suggested that the evolution of cloud clusters can be divided into four stages—formation, development, transition and cyclone formation—based on a study of medium-scale cloud clusters that developed over the western portion of the Baiu front (in China) and propagated to the Japanese Islands and the Pacific Ocean.

Several studies have noted the importance of convective forcing for the development of monsoon fronts and associated disturbances (e.g., Matsumoto et al., 1970; Wang and Orlanski,

Corresponding Author: Tae-Young Lee, Department of Atmospheric Sciences, Yonsei University, 50 Yonsei-Ro, Seodaemun-Gu, Seoul 120-749, Korea.
E-mail: lty@yonsei.ac.kr

1987; Tochimoto and Kawano, 2012; Jung and Lee, 2013). Wang and Orlanski (1987) found through a numerical study that, without latent heating, dynamic instability and/or forcing of the large-scale flow interaction with the Tibetan Plateau was not sufficient to generate a heavy-rain vortex originating on the lee side of the Tibetan Plateau. Matsumoto et al. (1970) suggested that the kinetic energy of an intermediate-scale disturbance (frontal cyclone over the Baiu front) was transformed from the kinetic energy of convective motion. Tochimoto and Kawano (2012) found through a composite analysis and case studies that latent heating played an important role in the development of western Baiu frontal depressions. Recently, Jung and Lee (2013) found that an ML that brought heavy rainfall to the Seoul area was initiated by mesoscale convective systems (MCSs) along the Changma front over the Yellow Sea.

Matsumoto et al. (1970) found that the thermal structure of a cyclone over the Baiu front was characterized by a cold lower troposphere and a warm upper troposphere within the cyclone region, and Yoshizumi (1977) found that two intermediate-scale disturbances developing on the Baiu front with a shallow vertical extension below the 400 hPa level were of the warm-core type. Tagami et al. (2007) categorized meso-α-scale disturbances that developed along the Baiu front in the year 2001 into two types: Type-1 disturbances, with a deep vertical trough that tilts westward with increasing height, and Type-2 disturbances, with a shallow vertical trough tilting eastward with increasing height.

Heavy rainfall events over the Korean Peninsula are often associated with MLs that originate in China and propagate eastward along the Changma front (Park et al., 1986; Lee and Kim, 2007), and cloud clusters are the most frequent type of heavy precipitation systems (HPSs) over the Korean Peninsula (Lee and Kim, 2007). Understanding of the MLs associated with the cluster-type HPSs can provide very useful knowledge for heavy rainfall forecasts. This is the motivation of the present study.

In this paper, an investigation is carried out to describe the locations of the initial occurrence, evolution and structure of MLs that are associated with cloud clusters and heavy rainfall over the Korean Peninsula during 2001-2010 using observation and reanalysis data. Section 2 describes disturbances associated with cloud clusters and heavy rainfall over the Korean Peninsula and the location of the initial ML occurrence. Section 3 discusses the synoptic-scale environment of ML initiation, followed by descriptions of the movement and evolution of MLs in Section 4. The structure of MLs at or near the time of heavy rainfall over the Korean Peninsula is analyzed in Section 5, and a summary and conclusions are provided in Section 6.

Table 1. Occurrence frequency of mesoscale depressions associated with heavy rainfall and cloud clusters over the Korean Peninsula during 2001-2010.

	Meso-α-scale low	Mesoscale trough	Not defined	Total
June	5	3	1	9
July	14	9	-	23
August	8	2	1	11
September	2	-	-	2
Total	29	14	2	45

2. Meso-α-scale lows associated with cloud clusters over the Korean Peninsula

a. Data and methods

In this section, we analyze observations and reanalysis data to 1) select heavy rainfall events associated with MLs that accompany cloud clusters, and 2) determine the location of initial ML occurrence for each event. The analysis is carried out for the summer season (June-September) from 2001. The data used in this study include synoptic observation data and automatic weather station (AWS) data; rawinsonde data; radar images; synoptic weather charts from the Korea Meteorological Administration; Multi-functional Transport Satellite (MTSAT) data; and National Centers for Environmental Prediction (NCEP) climate forecast system reanalysis (CFSR) ($0.5^o \times 0.5^o$ data) (Saha et al., 2010).

A heavy rainfall event is defined as a case with a 24-h rainfall amount greater than 80 mm at least at one station. Then, the selection of heavy rainfall events associated with cloud cluster is performed among heavy rainfall cases using rainfall data, satellite and radar images and the criteria used to define cloud cluster. In this study, we employ the criteria defining a cloud cluster used by Lee and Kim (2007): an oval-shaped cloud mass region of T_B (equivalent black-body temperature) lower than -50^oC is equal to or larger than 100 km in diameter. Flexibility concerning the shape is permitted, as indicated by Lee and Kim (2007). A cloud cluster may not exhibit an oval-shaped area of low cloud-top temperature in the satellite imagery; it may consist of several HPSs or meso-β-scale areas of convective rainfall embedded in a continuous stratiform precipitation area. Finally, the identification of mesoscale depression type associated with a cloud cluster for each selected heavy rainfall event was accomplished primarily using synoptic weather charts and NCEP CFSR data. Here, the term "mesoscale depression" includes MLs and mesoscale troughs, etc., and the term "mesoscale trough" is used for a depression which is not developed into a meso-α-scale closed isobar.

b. Selected cases

Forty-five heavy rainfall events associated with cloud clusters were selected (Table 1). As shown in this table, approximately two-thirds (29 of 45) of the events are associated with MLs, and 14 events are associated with mesoscale troughs (MTs),

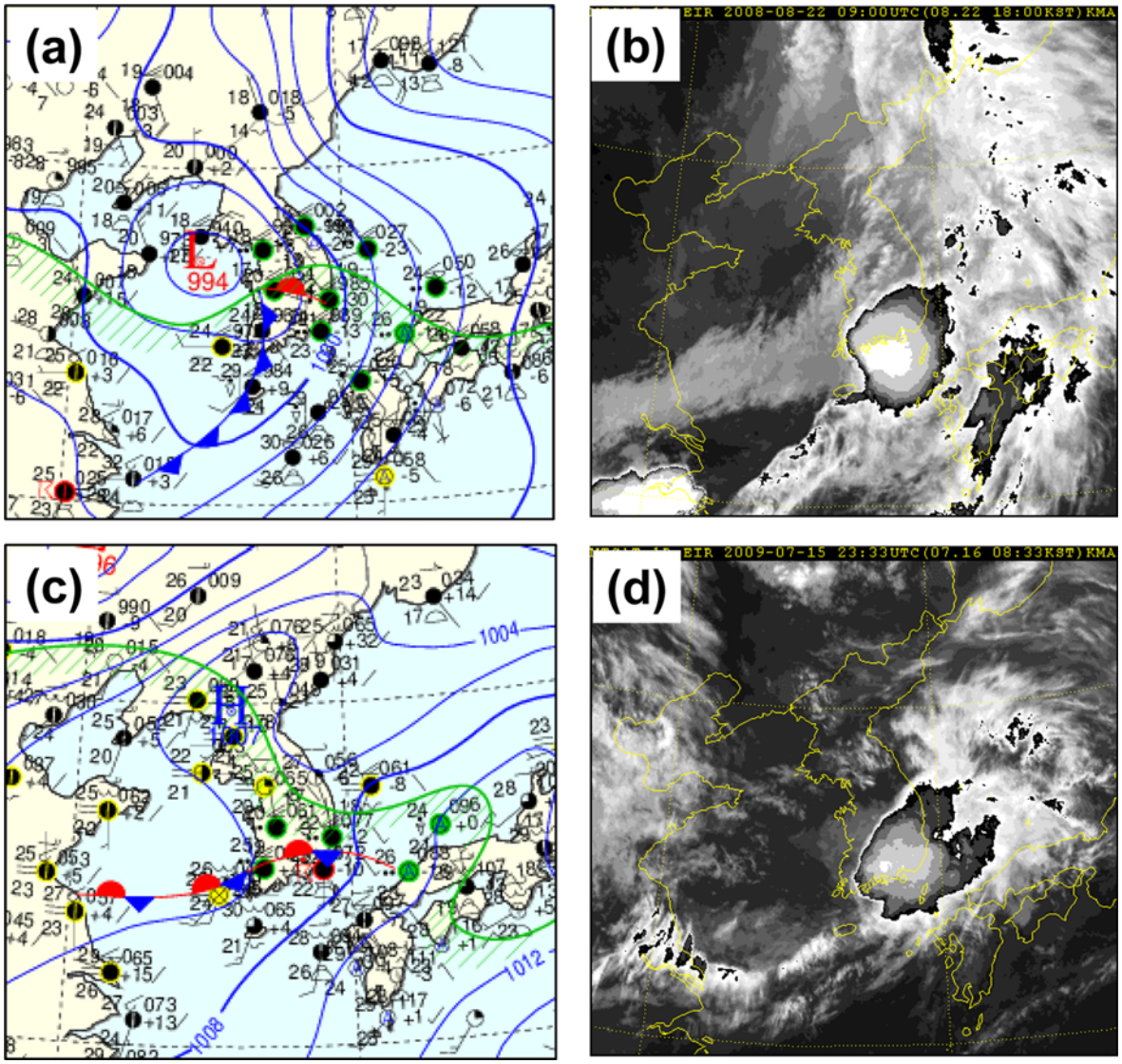

Fig. 1. Surface weather chart and enhanced IR images for (a, b) 0900 UTC 22 August 2008 and (c, d) 0000 UTC 16 July 2009. The satellite image in (d) is for 2333 UTC 15 July 2009.

whereas 2 events do not show any significant depression and are classified as "not defined". Examples of ML and MT cases are shown using surface weather charts and enhanced IR images in Fig. 1. Cloud clusters can be found in the southeastern part of an ML (Figs. 1a and b) and along an axis of an MT (Figs. 1c and d).

Examination of data indicates that MLs are mostly propagated from China and the western Yellow Sea, whereas MTs develop over the Yellow Sea and the west coast of the Korean Peninsula. Heavy rainfall associated with MTs may occur soon after the initiation of MT. In this study, we consider the 29 ML cases associated with cloud clusters. The MT cases are excluded in this study, because the prediction of heavy rainfall associated with MTs requires a good understanding of MT development which is not available at present.

c. Locations of initial occurrence of meso-α-scale lows

The location of the initial ML occurrence is traced back using the 850-hPa charts from NCEP CFSR ($0.5^o \times 0.5^o$ data) at 6-h intervals. The 850-hPa charts are used because the MLs of interest tend to be initiated in the lower troposphere below 700 hPa and are well represented at 850 hPa. As discussed in Section 4, the maximum area-averaged vorticity is most often found in the 850- to 700-hPa layer in the early stage of ML development. Relative vorticities at the 850- and 700-hPa levels are also used for the determination of the location of initial ML occurrence. The location of initial ML occurrence is defined as the position of the minimum height at the first appearance of a closed low with a diameter greater than 2^o, and after the first appearance, the low should maintain the closed-low shape until it reaches the Yellow Sea.

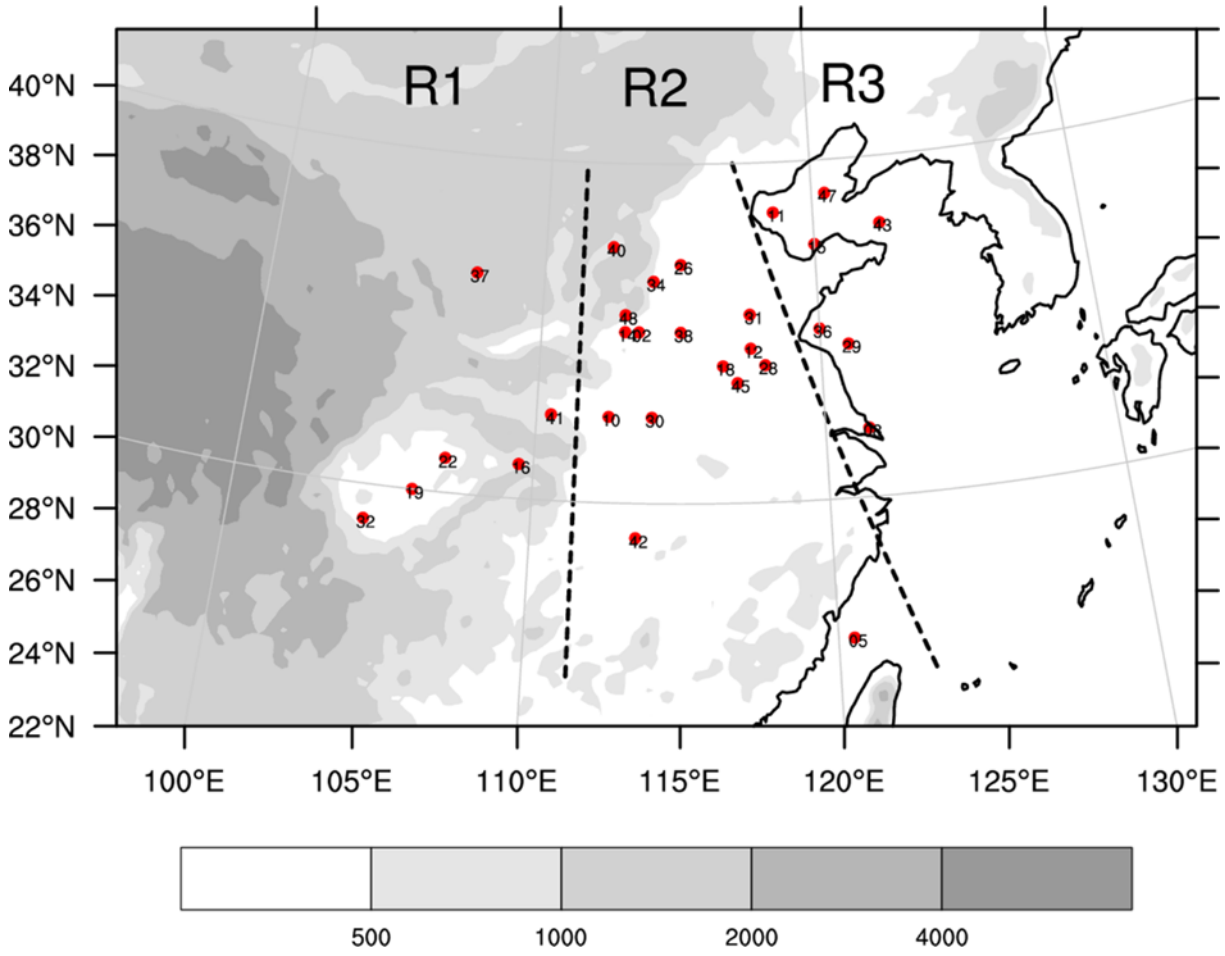

Fig. 2. Locations of initial appearance of meso-α-scale low. Shading represents terrain height (m), and numbers represent the case numbers.

Figure 2 shows the locations of initial ML occurrence of the 29 MLs identified in Table 1. The locations are widely spread from the east of the Tibetan Plateau to the Yellow Sea. These locations are clustered into three regional groups: the eastern flank of the Tibetan Plateau (referred to as region 1, R1), central and eastern China (R2) and the Yellow Sea (R3) (Fig. 2). Meso-α-scale lows first appear over R1 in 6 events, R2 in 16 events and R3 in 7 events. In terms of terrain, initial MLs are found over the Sichuan Basin and mountainous area to the east of the Tibetan Plateau with terrain height below 2 km in R1. In R2, they appear mainly over the plain of central and eastern China except for 3 cases (CC34, CC40, and CC48) over Taihangshan mountain range of north-central China.

This grouping of locations of initial ML occurrence is mainly to describe the average environment of ML generations with geographical proximity between the locations of initial ML occurrence within a group. It is also used to facilitate some descriptions of movements and evolution. Dynamical characterization of each region concerning ML initiation and development is not attempted in this study. The regions may be under various influences of dynamical and physical factors including mountains [e.g., the Tibetan Plateau (e.g., Wang and Orlanski, 1987) and the Yanshan-Taihangshan mountain ranges (e.g., Bao and Zhang, 2013)] and land use (e.g., Shinoda and Uyeda, 2002) in an environment of large scale monsoon circulations such as the WPSH and Mei-yu/Changma fronts. Dynamical characterization may require a comprehensive understanding of those influences.

3. Environment of initial meso-α-scale lows

In this section, the environment for initial ML occurrence is examined using composite charts at 850-, 500- and 300-hPa levels. Composite charts are generated for the time of initial ML appearance in each region group. The charts for the R2 group are obtained using 15 cases, excluding CC05, in which an ML is initiated over the ocean area to the north of Taiwan.

Composite charts for the 3 groups are shown in Fig. 3. A characteristic large-scale height pattern for whole groups is shown at 850 hPa, in which a broad trough exists over much of China between the western Pacific subtropical high (WPSH) and the Tibetan Plateau (Figs. 3a, c, and e). The trough extends

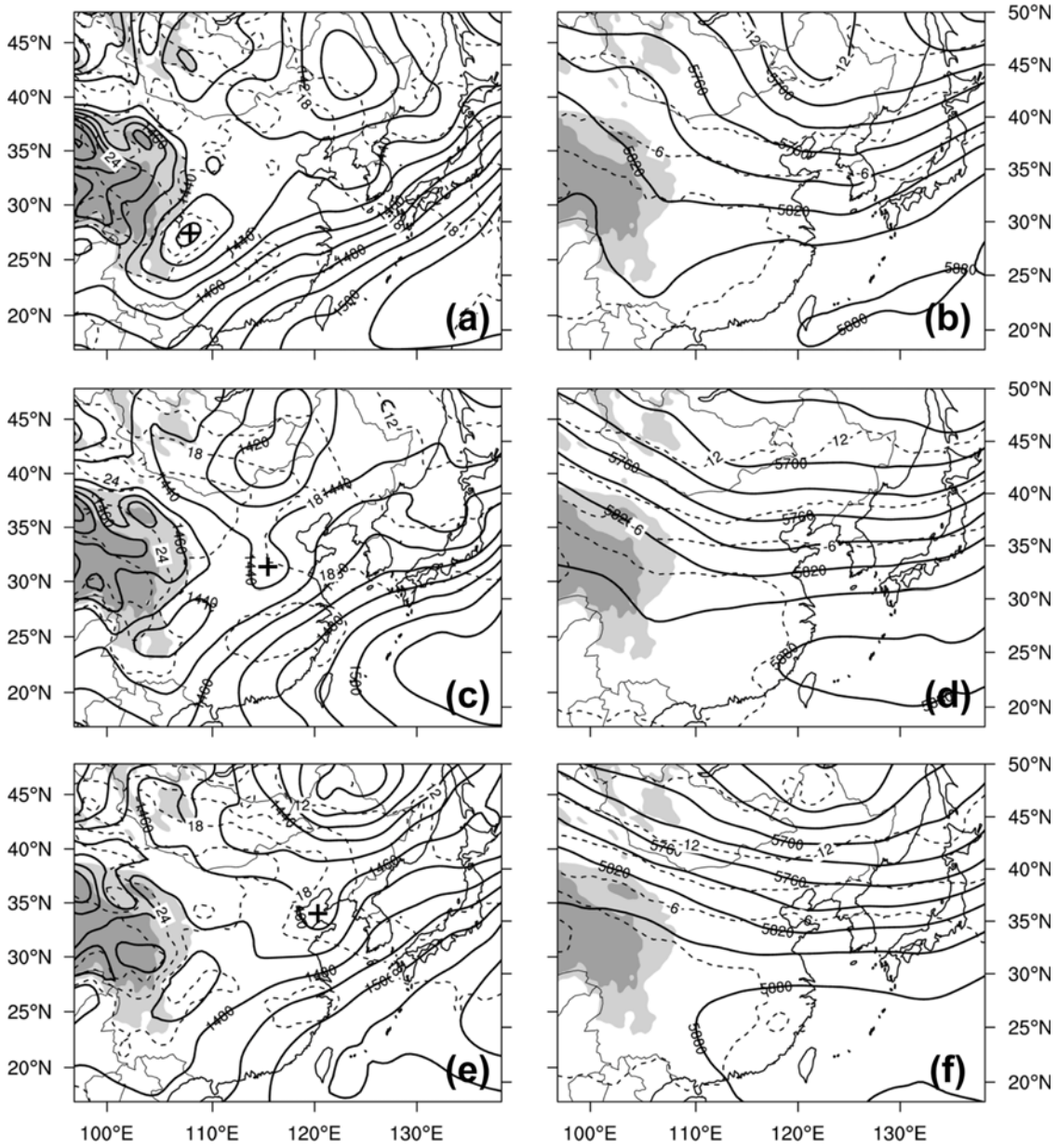

Fig. 3. Composite charts for 850 hPa (left panels) and 500 hPa (right panels) at the time of initial occurrence of a mesoscale low for the (a, b) R1, (c, d) R2, and (e, f) R3 groups. Solid and dashed lines represent geopotential height (m) and temperature (°C), respectively. Mesoscale trough or low center at 850 hPa is marked by "+". The boundaries of light and dark shadings represent terrain contours of 2000 and 4000 m, respectively.

from the southeast of the Tibetan Plateau to northern or northeastern China, where a synoptic-scale cyclone is located. A meso-α-scale low is found at 850 hPa to the southeast of the Tibetan Plateau in all groups. Another important common feature is that the horizontal temperature gradient at 850 hPa is weak over the area of ML occurrence.

Some distinct features for each regional group can also be found. The composite charts for the R1 group show a trough along the eastern flank of the Tibetan Plateau throughout the middle to lower troposphere with a northwest tilt (Figs. 3a and b). A well-defined ML is found to the southeast of Tibetan Plateau (marked by "+" in Fig. 3a). The composite 850-hPa chart for the R2 group shows a mesoscale trough over central China in between the Tibetan Plateau and the Shandong Peninsula (marked by "+" in Fig. 3c). The trough is located within a long trough extended from the southeast of the Tibetan Plateau to a synoptic-scale cyclone over northern China. At 500 hPa, a weak trough is found upstream of the mesoscale trough at 850 hPa (Fig. 3d). In the R3 group, a mesoscale trough is found over the Shandong Peninsula, with its axis oriented in a NW-SE direction (marked by "+" in Fig. 3e). A broad trough with its center over northeastern China is

indicated at both levels, with no noticeable features at 500 hPa above the area of ML formation (i.e., the western Yellow Sea) (Fig. 3f).

The present analysis indicates that initial MLs tend to occur within a deep trough over the eastern flank of the Tibetan Plateau (R1 cases) or a long trough extended northeastward from the southeast of the Tibetan Plateau along the northwestern rim of the WPSH (a majority of R2 cases and two R3 cases).

4. Movement and evolution of meso-α-scale lows

a. Movements

Tracks of ML movement are shown for each regional group in Fig. 4. A track is generated by connecting the positions of ML centers (marked by dots in Fig. 4) at 6-h intervals. In the R1 group, MLs tend to move northeastward, reaching the northern or middle Korean Peninsula, except for one case (Fig. 4a). Meso-α-scale lows in the R2 group show either northeastward or east-northeastward movement, reaching the northern and southern Korean Peninsula (Fig. 4b). In the R3 group, MLs tend to show eastward movements except for two cases (Fig. 4c).

The speed of ML movement varies with each case and with the location of ML. The average speeds of ML movement from the initial occurrence to arrival near the west coast of the Korean Peninsula are 32.4, 37.2 and 40.4 km h^{-1} for the R1, R2 and R3 groups, respectively. Examination of tracks reveals a tendency of slow movements in the early stage in 3 cases of the R1 group (Fig. 4a) and in the stage of approaching the Korean Peninsula in several cases of the R1 and R2 groups (Figs. 4a and b). Thus, the average speed of each ML shows a large variation, ranging from 19.4 to 56.9 km h^{-1}. Akiyama (1984) found that the cloud cluster generated at the eastern foot of Tibetan Plateau propagated eastward with a phase speed of ~1000 km day^{-1} (approximately 42 km h^{-1}), which is within the speed range of this study.

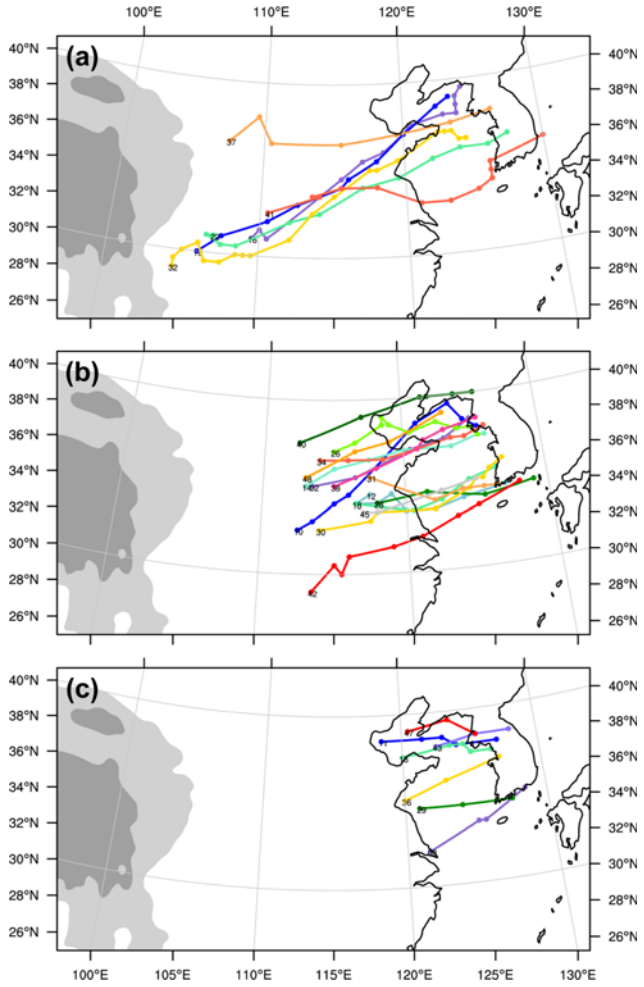

Fig. 4. Tracks of meso-α-scale low center for the (a) R1, (b) R2, and (c) R3 groups. Shading represents terrain, as in Fig. 3.

Direction of ML movement appears to depend on the manner of the WPSH development toward the eastern Asia and also the southward development of a synoptic-scale cyclone over northern or northeastern China. Figure 5 shows

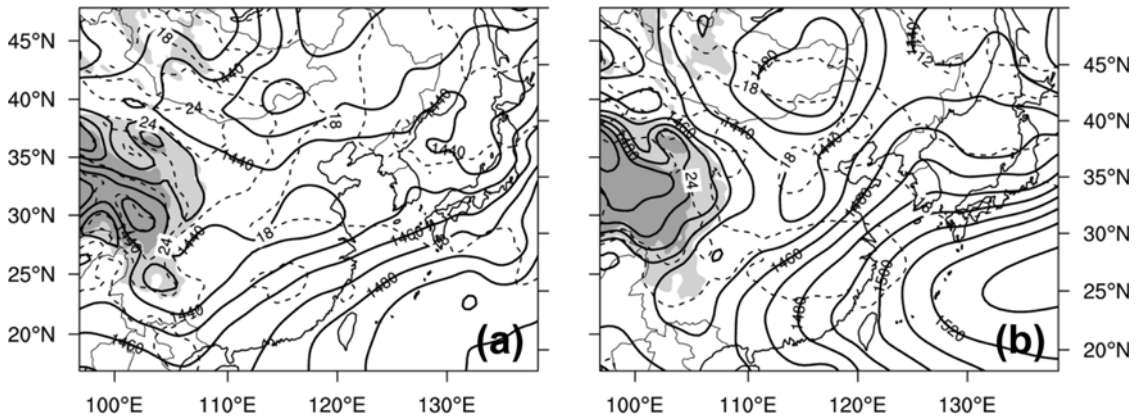

Fig. 5. Composite charts for 850 hPa height fields at the time of initial ML occurrence in R2 for the groups of MLs moving toward (a) the southern Korean Peninsula and (b) the northern Korean Peninsula. Shading represents the terrain, as in Fig. 3.

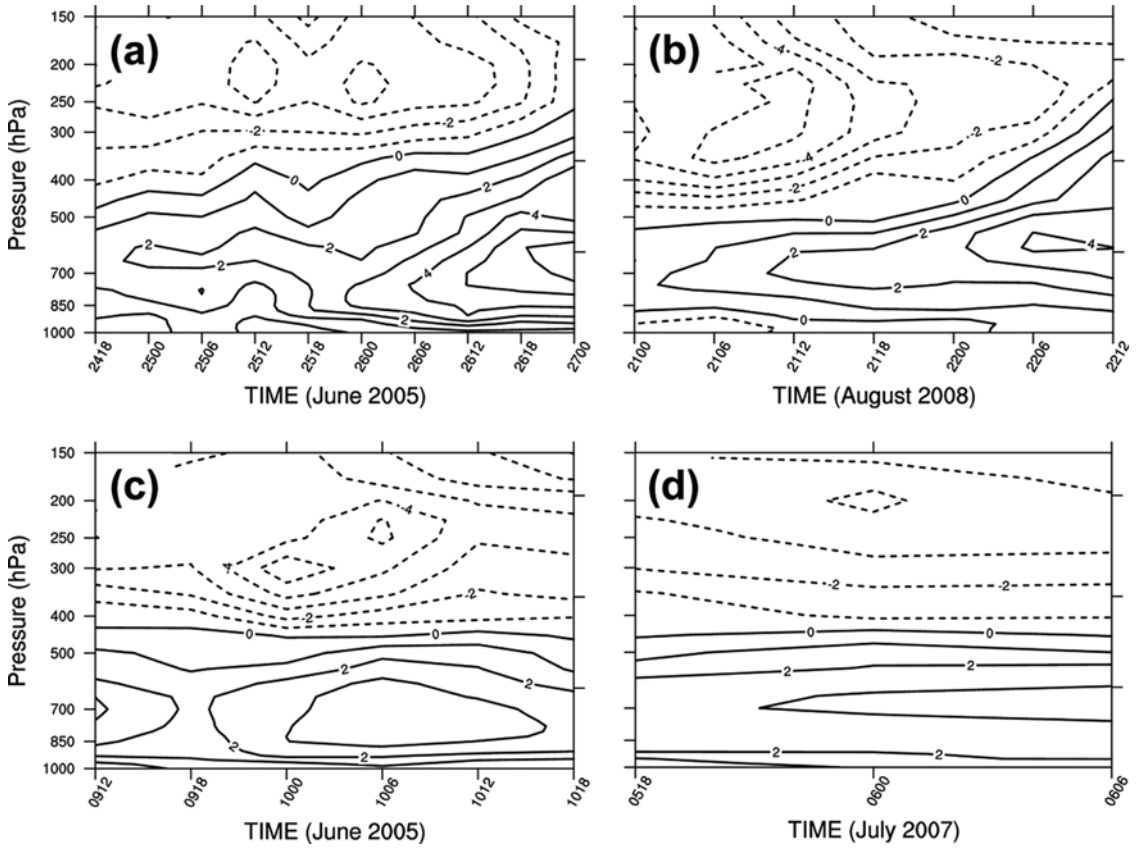

Fig. 6. Temporal evolution of area-averaged relative vorticity ($\times 10^{-5}$ s^{-1}) for two cases from each origin group: (a) R1-CC19, (b) R2-CC34 (c) R2-CC18 and (d) R3-CC29. Area averaging is carried out for an area of $6^o \times 6^o$, centered on the ML center. The average vorticity is shown from the time of initial occurrence to the time when the ML center passes over the Korean Peninsula or stagnates near the west coast of the Korean Peninsula.

the composite charts for 850-hPa height fields at the time of initial ML occurrence in R2 for the groups of ML moving toward the southern Korean Peninsula (Fig. 5a) and the northern Korean Peninsula (Fig. 5b). Directions of contour along the northwestern rim of the WPSH in Figs. 5a and 5b match well with the paths of MLs moving toward the southern and northern Korean Peninsula in Fig. 4b, respectively. Similar results are also obtained for the MLs in the R1 group (not shown). Such dependence of ML movement can also be found later in individual cases in Figs. 7, 8, 9, and 10.

b. Evolution

Evolution of meso-α-scale low is examined using a time-height cross section of vertical component relative vorticity averaged over an area of $6^o \times 6^o$ on the ML center, from the initial ML occurrence to the time of the ML reaching the west coast of the Korean Peninsula or stagnating over the Yellow Sea near the coast. These cross sections are generated for all 29 events considered in this study.

Vertical structure of area-averaged vorticity associated with MLs may be characterized by layers of cyclonic and anti-cyclonic vorticity in the lower and upper troposphere, respectively (Fig. 6). The top height of cyclonic-vorticity layer may increase with time (Figs. 6a and b) or remain steady (Figs. 6c and d). It increases with time mainly when upper-level trough approaches the ML from the west or northwest, but tends to remain steady when MLs are away from the downstream of upper-level trough (e.g., in the upstream of a trough). Half of the cases in R1 and R2 groups exhibit steady top heights, while the other half shows temporal increase of the height. Here, steady cases include the cases in which the top heights vary less than 100 hPa. All of the R3 cases show steady top mainly because travel time is relatively short. The four cases shown in Fig. 6 belong to these evolution patterns: non-steady cases (Figs. 6a and b) and steady cases (Figs. 6c and d). Initial occurrence and movement of an ML for each case of Fig. 6 are shown in Figs. 7, 8, 9, and 10.

In the CC19 case, an ML appears to the southeast of the Tibetan Plateau at 0000 UTC 25 June 2005 and moves northeastward reaching the northern Yellow Sea at 1800 UTC 26 June (Fig. 7). As indicated by the equivalent black-body temperature measured by the MTSAT in Fig. 7, the ML is accompanied by deep MCSs throughout its life. It is generated in a deep layer of cyclonic vorticity, whose initial top is just above the 500-hPa level (Fig. 6a). In the initial stage, the

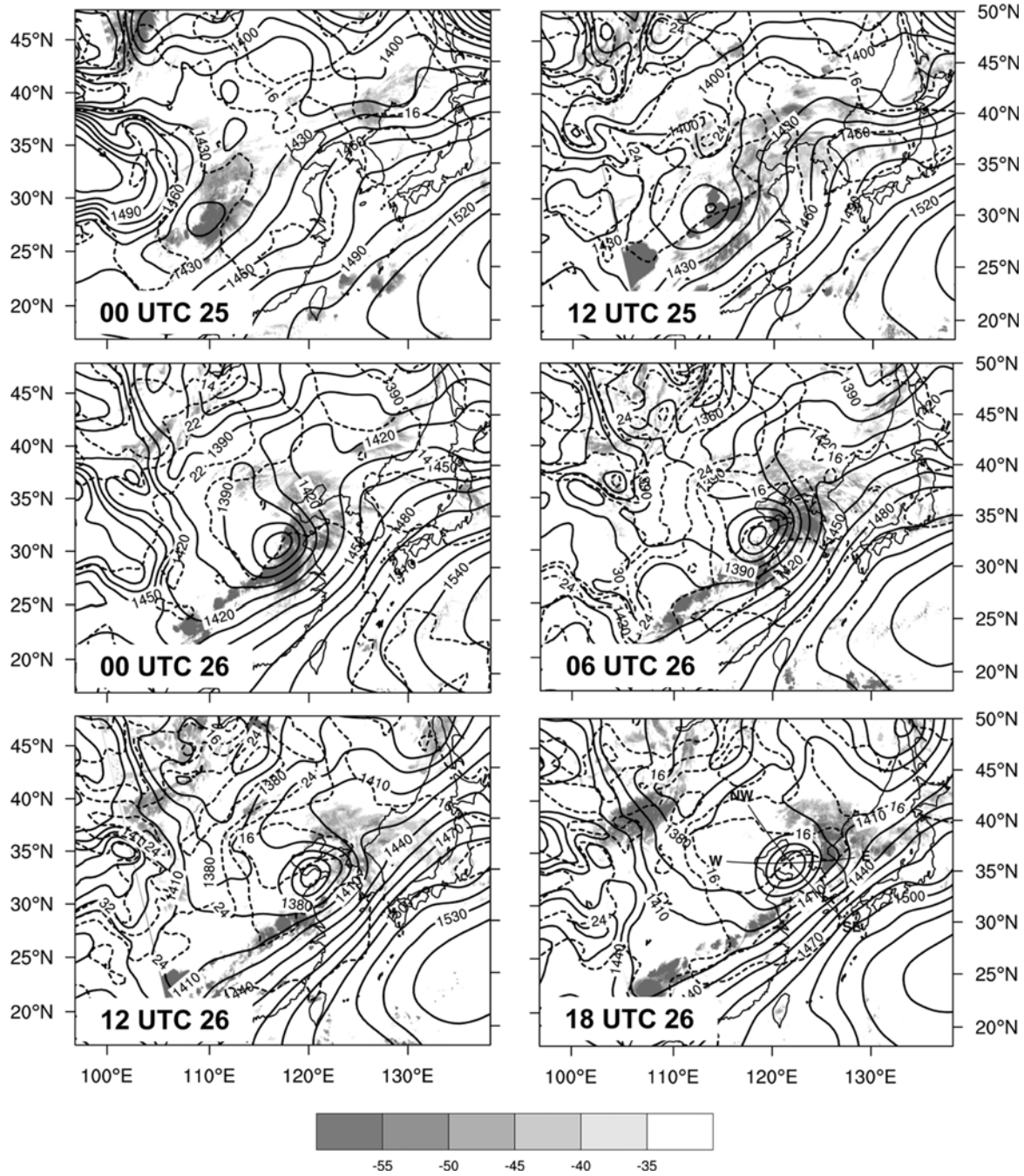

Fig. 7. The 850-hPa constant pressure charts: height (m, solid lines) and temperature (°C, dashed lines) during 0000 UTC 25-1800 UTC 26 June 2005 (R1-CC19). Shading indicates the equivalent black-body temperature measured by the MTSAT. The thin solid lines across the ML center for 1800 UTC 26 June indicate the locations of cross section in Figs. 11a and b.

maximum vorticity is found in between 700- and 600-hPa levels. Vorticity does not exhibit notable variation with time in this stage. A relatively fast increase of vorticity is found near the 850 hPa level after 1200 UTC 25 June as the ML deepens considerably while moving toward the Shandong Peninsula (Fig. 6a and Fig. 7). The maximum vorticity of 3×10^{-5} s^{-1} is indicated at approximately 850 hPa at 0000 UTC 26 June. Both vorticity and the level of maximum vorticity increase after 0600 UTC 26 as the ML moves to the northern Yellow Sea, passing the Shandong Peninsula. At 0000 UTC 27 June, the depth of cyclonic-vorticity layer has extended up to the upper troposphere (above 300 hPa). Similar pattern of evolution in the early period (i.e., initial maximum vorticity at levels above 700 hPa is followed by a development near 850 hPa) can be found only in 3 cases of the R1 group.

In the CC34 case, an ML forms over central China at about

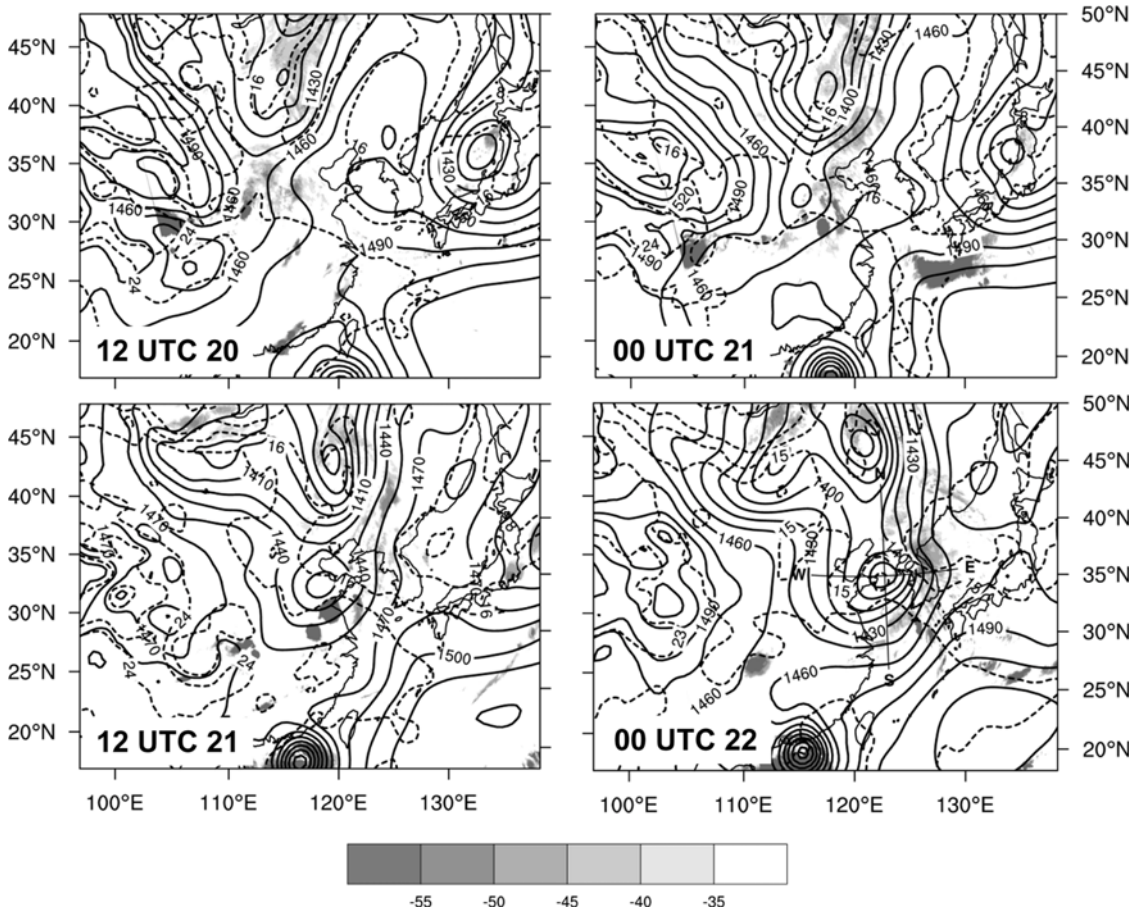

Fig. 8. Same as Fig. 7, except for 1200 UTC 20-0000 UTC 22 August 2008 (R2-CC34). The thin solid lines across the ML center for 0000 UTC 22 August indicate the locations of the cross section in Figs. 11c and d.

0000 UTC 21 August 2008 and moves eastward (Fig. 8). After 0000 UTC 22 August, it moves very slowly over the Yellow Sea approaching the west coast of the Korean Peninsula (not shown). In this case, vorticity and the level of its maximum increase slowly with time until 0000 UTC 22 August 2008, whereas the depth of cyclonic vorticity layer remains steady below 500 hPa (Fig. 6b). Both the cyclonic vorticity layer and the maximum vorticity grow relatively fast after 0000 UTC 22 August, as the ML stagnates and upper-level trough approaches the ML from the northwest.

In the CC18 case, an ML forms to the southwest of the Shandong Peninsula and moves eastward approaching the southwestern coast of the Korean Peninsula at 0600 UTC 10 June 2005 (Fig. 9). This case exhibits a nearly constant top height of the cyclonic vorticity layer (Fig. 6c). And the level of vorticity maximum is also maintained near 850 hPa. Vorticity reaches the maximum at 0600 UTC 10 June, and then decreases with time as the ML moves over the southern Korean Peninsula.

In the CC29 case, an ML appears over the Yellow Sea near the Chinese coast at approximately 1800 UTC 5 July 2007 and moves to the southern coast of the Korean Peninsula at 0600 UTC 6 July (Fig. 10). During this period, the top of the cyclonic vorticity layer is maintained in the middle of the 500- to 400-hPa layer (Fig. 6d). An increase in vorticity at 700 hPa can be seen during the movement.

Approximate symmetries of positive and negative vorticity distribution are present between the lower and upper troposphere in the CC18 and CC29 cases (Figs. 6c and d). These features may be similar to Akiyama's (1984) findings that kinematic properties of a cloud cluster are a medium-scale cyclonic circulation in the lower troposphere just behind (west side of) the cloud cluster and an anticyclonic circulation in the upper layer over the cloud cluster.

Evolutions of area-averaged vorticity in 27 cases are summarized in Table 2. In this statistics, two cases are excluded due to a large temporal variation of cyclonic vorticity layer (CC05) or a structure with positive vorticity through whole troposphere (CC26). The top of the cyclonic vorticity layer is found mainly below 400 hPa at the time of initial ML occurrence, and it is still below 400 hPa in majority of cases (18 cases) at the time of ML over the Yellow Sea, when heavy rainfall may occur over the Korean Peninsula. The maximum vorticity is most frequently located in the layer 850-700 hPa at the time of initial ML, but it is almost evenly distributed in the two layers of 700-500 hPa and 850-700 hPa at the time of ML

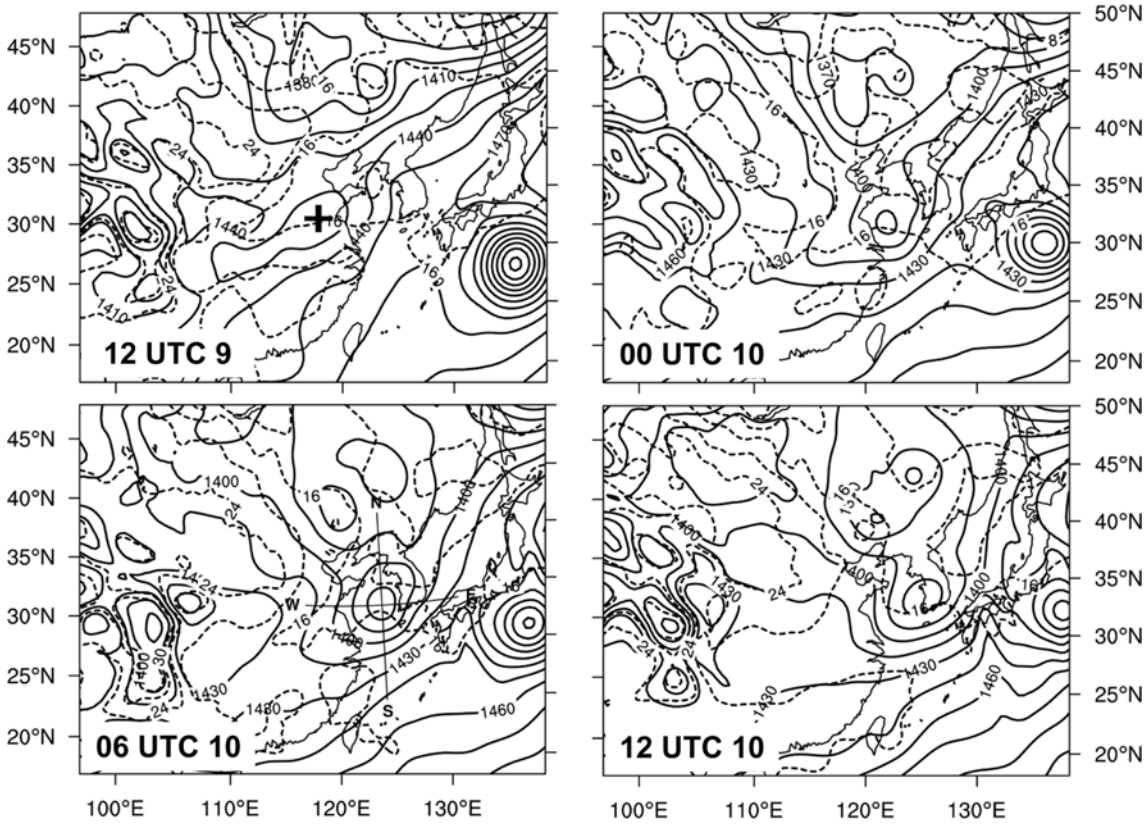

Fig. 9. Same as Fig. 7, except for 1200 UTC 9 - 1200 UTC 10 June 2005 (R2-CC18). The thin solid lines across the ML center for 0600 UTC 10 June indicate the locations of the cross section in Figs. 11e and f. The equivalent black-body temperature is not shown here due to the absence of the MTSAT data.

over the Yellow Sea. This result indicates that initial MLs tend to develop in the lower troposphere below 700 hPa, and some of them grow vertically.

5. Structure of meso-α-scale lows near the Korean Peninsula

In this section, we describe the structure of MLs at or near the time of heavy rainfall over the Korean Peninsula for the cases considered in the previous section (i.e., the four cases in Fig. 6).

a. Vertical structure

Vertical structure of an ML is described using temperature and height perturbations in cross sections across the ML center at 850 hPa at or near the time of heavy rainfall over the Korean Peninsula, when MLs are located mostly over the Yellow Sea. Perturbation is defined as a deviation from the horizontal average along a cross section. Two cross sections are obtained for each case: a cross section along the direction of vertical tilt of ML center and an E-W cross section. The length of the cross section extends across 17° of longitude (latitude) for an E-W (N-S) cross section, or approximately the same length for cross sections in other direction.

Figure 11 shows the vertical structure of the four MLs shown in Figs. 7, 8, 9, and 10. The ML of the CC19 case at 1800 UTC 26 June 2005 is found to have a northwestward tilt with height (Fig. 11a). The cross section in the NW-SE direction shows that negative height perturbation, including the ML in the lower half of the troposphere, is tilted northwestward throughout the troposphere as cold anomaly is located to the northwest of the ML center (Fig. 11a). Perturbation structures in the E-W cross section are similar to those in the NW-SE cross section, since the directions of the two cross sections differ by 45° (Fig. 11b). The ML shows a warm-core thermal structure. Overall pattern of temperature perturbation exhibits cooler air in the west and warmer air over and in the east of the ML center. A lag between the thermal and height troughs is also indicated, as for a baroclinic low-pressure system. Upper-air charts for the same time are shown in Figs. 12a and 12b. The synoptic-scale trough shows a westward tilt with height, and the lag between the 500- and 850-hPa troughs is substantial. The ML is tilted toward the eastern part of the synoptic-scale low at 500-hPa (Fig. 12a).

Meso-α-scale low of the CC34 case at 0000 UTC 22 August 2008 is found to have an eastward tilt (Figs. 11c and d). Meridional gradient of height perturbation is strong in the upper troposphere especially over 39°-41°N, while it is very weak in the lower troposphere to the north of the ML (Fig.

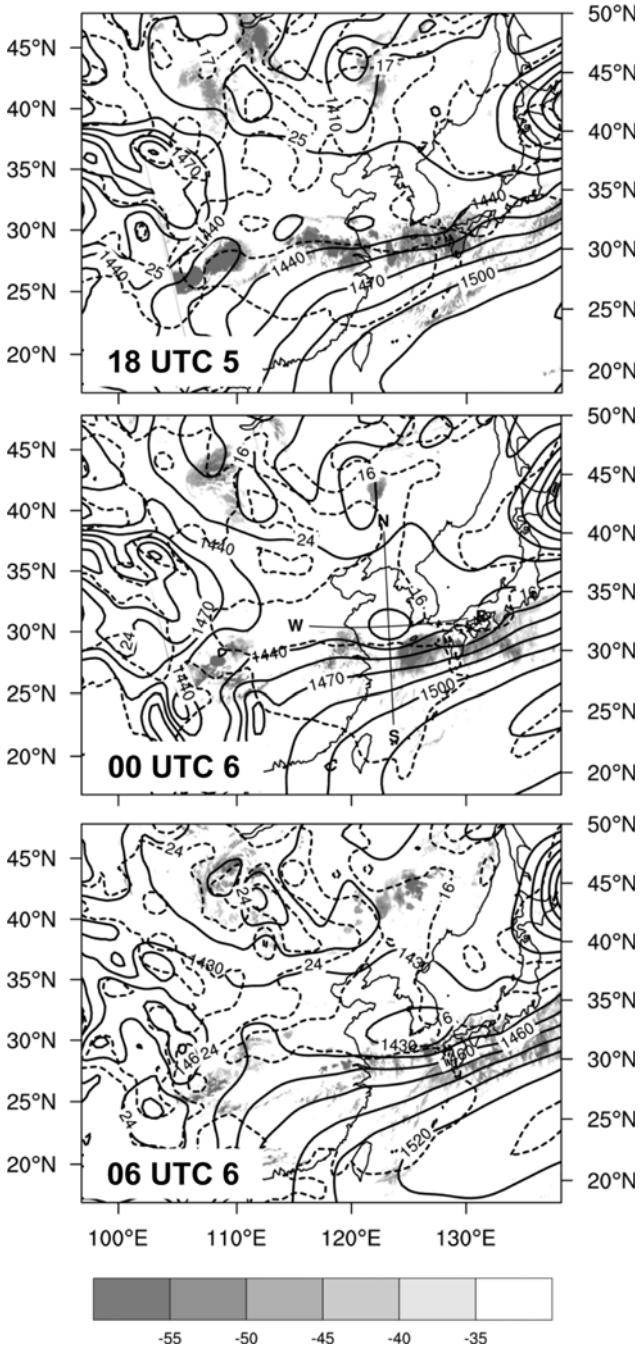

Fig. 10. Same as Fig. 7, except for 1800 UTC 5 - 0600 UTC 6 July 2007 (R3-CC29). The thin solid lines across the ML center for 0000 UTC 6 July indicate the locations of the cross section in Figs. 11g and h.

11c). A strong cold anomaly is found at low levels over the northern side of the ML. The ML, below about 500 hPa at the 37.5° latitude, is nearly vertical except for a slight northward tilt below 800 hPa. In the E-W cross section, the ML center is tilted eastward with height above 800 hPa (Fig. 11d). This eastward tilt may be due to the presence of cooler air below 500 hPa on the eastern side of the ML. It may be said that the warm-core ML in this case is tilted slightly northward below

Table 2. Occurrence frequency of the top height of cyclonic vorticity layer and the level of maximum vorticity at the time of initial ML occurrence and the time of ML over the Yellow Sea, when heavy rainfall may occur over the Korean Peninsula.

	Level (hPa)	Time of initial ML occurrence	Time of ML over the Yellow Sea
Top of cyclonic vorticity layer	Above 300	-	4
	400 - 300	4	5
	500 - 400	13	14
	700 - 500	10	4
Level of maximum vorticity	700 - 500	6	13
	850 - 700	19	14
	Below 850	2	-

800 hPa and then eastward between 800 and 500 hPa. Upper-air chart for 500 hPa at the same time show the presence of two troughs: one upstream and a minor one immediately downstream of the ML (Fig. 12c). The minor trough at downstream is consistent with the eastward tilt of the ML in Fig. 11d. Another important feature is indicated at low levels to the east of the ML center, where a strong cold anomaly exists (Fig. 11d). Reanalysis indicates that the cold anomaly may represent the cooler air within the thermal trough extended from the northeast toward the Yellow Sea (Fig. 8). It is also possible that this cold anomaly may be enhanced by either evaporative cooling of rainwater or adiabatic cooling resulted from a strong updraft. Tagami et al. (2007) found a similar cold anomaly at low levels and suggested that it was caused by adiabatic cooling associated with the strong updraft induced by condensational heating in the mid and upper levels.

In the CC18 case, the ML at 0600 UTC 10 June 2005 is found to have a significant northward tilt (Fig. 11e). Vertical structures in the N-S cross section are similar to those of the previous case (i.e., CC34), except that negative temperature perturbation is found below the ML. This cold anomaly below the ML seems to be associated mainly with the synoptic-scale thermal trough extended to the Yellow Sea from Okhotsk Sea (Fig. 9). The ML propagates toward the thermal trough over the Yellow Sea and becomes surrounded by cooler air. In the E-W cross section, it is nearly vertical with westward and eastward tilts below and above 850 hPa, respectively (Fig. 11f). Cold anomaly is found at low levels in both sides of the ML center. Upper air charts indicate that the ML is under the southern side of a broad upper-level trough, where a mesoscale thermal ridge can be found at 500 hPa over the ML area (Figs. 12e and f).

The meso-α-scale low of the CC29 case at 0000 UTC 6 July 2007 is also tilted northward with height (Fig. 11g). However, it is much weaker than the other MLs analyzed here (Fig. 11h). Perturbation structures in the E-W cross section in this case show some differences from the other three cases. Negative height perturbation is tilted eastward with height above 700 hPa, and warmer and cooler air can be found on the western

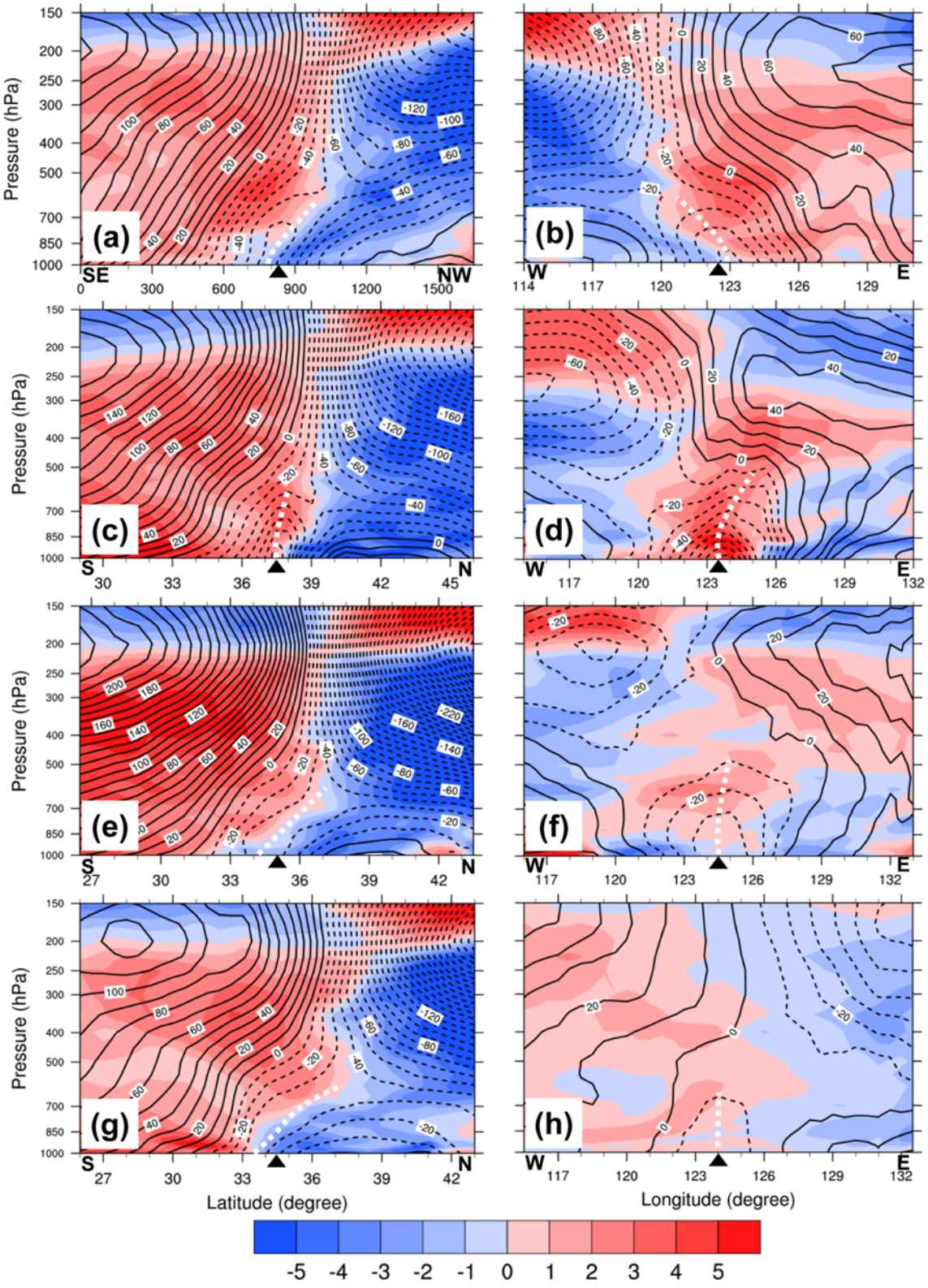

Fig. 11. Vertical cross sections of height deviation (m, solid and dashed lines for positive and negative deviations, respectively) and temperature deviation (°C, shaded) in the N-S (or NW-SE) direction (left panels) and the E-W direction (right panels) for (a, b) 1800 UTC 26 June 2005 (R1-CC19), (c, d) 0000 UTC 22 August 2008 (R2-CC34), (e, f) 0600 UTC 10 June 2005 (R2-CC18), and (g, h) 0000 UTC 6 July 2007 (R3-CC29). White dashed line and black triangle indicate the vertical trough and the position of ML center at 850 hPa, respectively. The location of each cross section is given in the 850 hPa chart for the given case and time in Figs. 7-10.

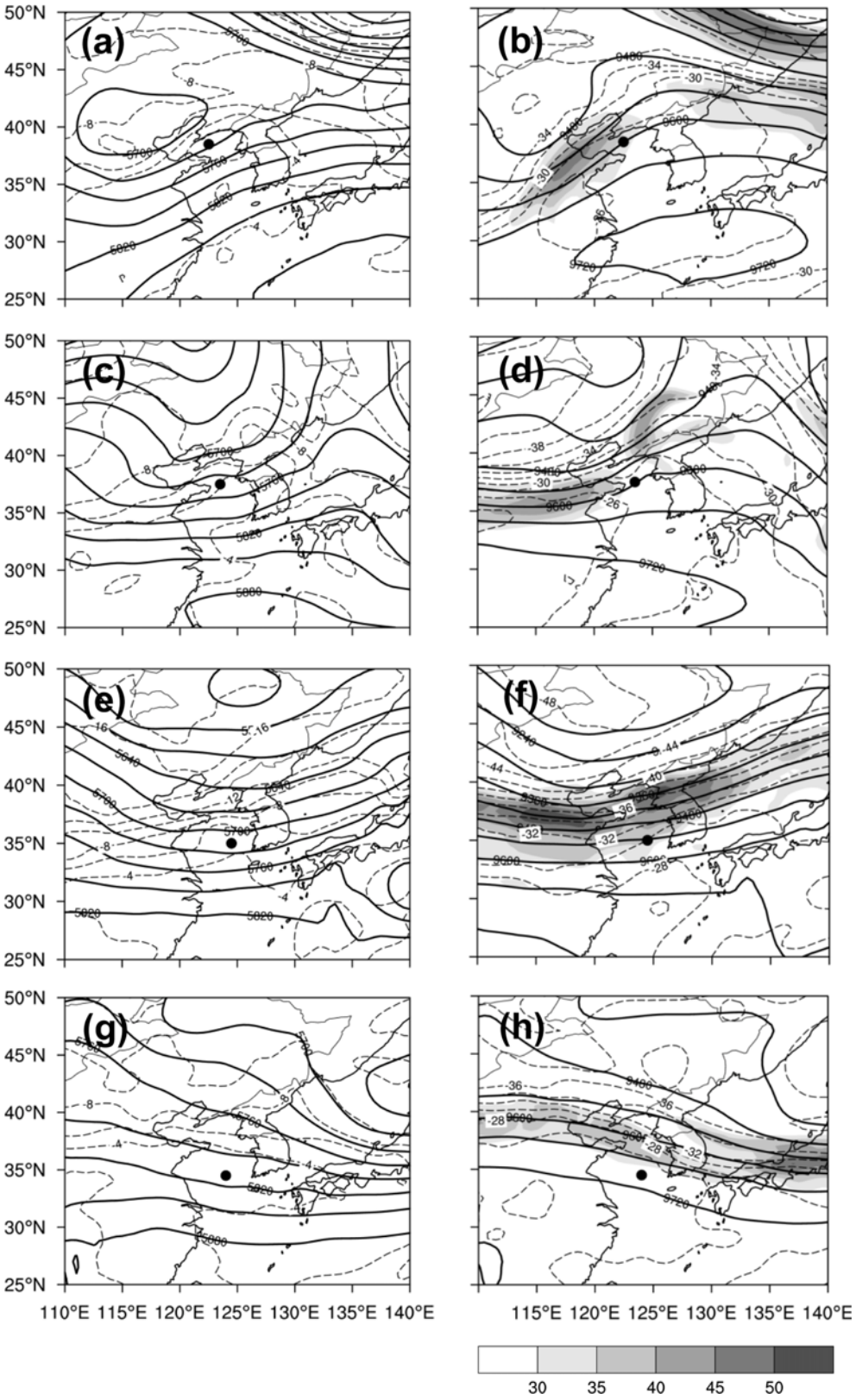

Fig. 12. The 500-hPa (left panels) and 300-hPa (right panels) charts from CFSR data for (a, b) 1800 UTC 26 June 2005 (R1-CC19), (c, d) 0000 UTC 22 August 2008 (R2-CC34), (e, f) 0600 UTC 10 June 2005 (R2-CC18), and (g, h) 0000 UTC 6 July 2007 (R3-CC29). Solid and dashed lines represent geopotential height (m) and temperature (°C), respectively. Shading for the 300-hPa chart indicates wind speed (m s^{-1}). Dots indicate the positions of 850-hPa ML centers.

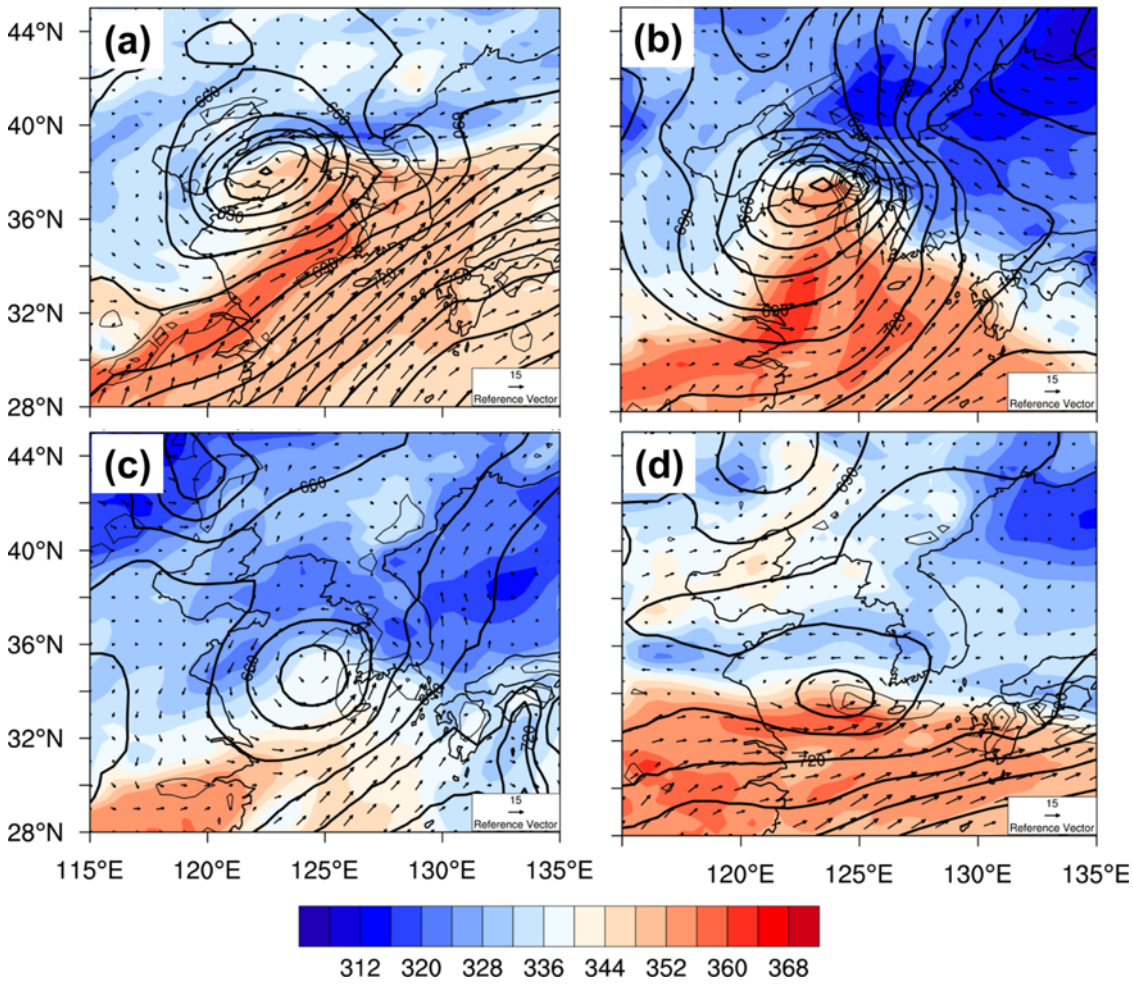

Fig. 13. Geopotential height (m, heavy solid lines), wind vector (m s^{-1}), and equivalent potential temperature (K, shaded) at 925 hPa for (a) 1800 UTC 26 June 2005 (R1-CC19), (b) 0000 UTC 22 August 2008 (R2-CC34), (c) 0600 UTC 10 June 2005 (R2-CC18), and (d) 0000 UTC 6 July 2007 (R3-CC29). Light solid lines indicate divergence smaller than -5×10^{-5} s^{-1} (contour interval is -10^{-4} s^{-1}).

and eastern sides of the ML, respectively (Fig. 11h). These features are in opposite sense to those for the other three cases shown in Fig. 11. Upper-level charts for this case do not show any notable features above the ML (Figs. 12g and h).

Analysis of vertical tilt of ML center for all the cases has revealed that ML is tilted northward in 14 cases, northeastward in 4 cases, northwestward in 4 cases, eastward in 2 cases, westward in 1 case, and nearly vertical in 4 cases. And MLs show warm-core thermal structure in general. As found in Fig. 11, vertical tilt of an ML depends on thermal structure around the ML, since height perturbation depends on temperature structure through hydrostatic relationship. It is also found that environment of ML (e.g., the synoptic-scale thermal trough) is an important factor for the vertical structure of MLs over the Yellow Sea.

b. Horizontal structure

The horizontal structures of the MLs at 925 hPa are shown in Fig. 13. The meso-α-scale lows exhibit a common pattern of digging into the WPSH, which strengthens the height gradient and winds on their southeastern sides. As a result of these wind structures, high-θ_e air penetrates into these areas and near the ML center. Note that high-θ_e air is found to the east of ML center in CC19 (Fig. 13a), while low-θ_e air exists there in CC34 (Fig. 13b). These are also noted in Figs. 11b and d.

A strong convergence zone is present near the northern end of the LLJ (or strong southwesterly) in all 4 cases shown in Fig. 13. Cloud clusters are found to develop over these convergence zones, into which a large amount of moisture is continuously transported by the southwesterly. The occurrences of deep convective systems in the eastern or southeastern parts of the MLs are also observed in Figs. 7, 8, and 10. Note that convergence zones extend eastward in the east of ML centers and may cause heavy rainfall over the Korean Peninsula when the MLs are still at a considerable distance from the Korean Peninsula.

Observations also indicate that eastern part of ML is the

favored site of cloud cluster development along the Mei-yu and Baiu fronts (Akiyama, 1984; Yang et al. 2010, and etc.). Heavy rainfall may occur in other parts of the low (e.g., Zhang et al., 2014). In the present study, all cloud clusters develop in the eastern part (including the southeastern part) of MLs. Some cases show heavy precipitation systems in the western part of ML. However, they do not satisfy the definition of cloud cluster.

6. Summary and conclusions

An investigation was conducted to describe the locations of initial occurrence, evolution and structure of MLs associated with cloud clusters and heavy rainfall over the Korean Peninsula using observation and reanalysis data. We examined 29 heavy rainfall cases associated with MLs that accompany cloud clusters during the 10-year period of 2001-2010.

The locations of initial ML occurrence are widely spread from the eastern flank of the Tibetan Plateau to the Yellow Sea. In this study, these locations are grouped into 3 regions: (1) the eastern flank of the Tibetan Plateau (R1, 6 cases), (2) central and eastern China (R2, 16 cases), and (3) the Yellow Sea (R3, 7 cases).

The environment of initial ML occurrence is examined using composite charts for each regional group. The composite charts exhibit a characteristic large-scale height pattern at 850 hPa for whole groups; a broad trough exists over much of China between the WPSH and the Tibetan Plateau. The trough extends from the southeast of the Tibetan Plateau to northern or northeastern China, where a synoptic-scale cyclone is located. Another important common feature is that the horizontal temperature gradient at 850 hPa is weak over the area of initial ML occurrence. Initial MLs tend to occur within a deep trough over the eastern flank of the Tibetan Plateau (R1 cases) or a long trough extended northeastward from the southeast of the Tibetan Plateau along the northwestern rim of the WPSH (a majority of R2 cases and two R3 cases).

Meso-α-scale lows tend to move northeastward, reaching the northern and middle Korean Peninsula in the R1 group; either northeastward or east-northeastward, reaching the northern and southern Korean Peninsula in the R2 group; and eastward in the R3 group. The average speeds of ML movement from the initial occurrence to arrival near the west coast of the Korean Peninsula are 32.4, 37.2 and 40.4 km h^{-1} for the R1, R2 and R3 groups, respectively.

The evolution of an ML is described using a time-height cross section of vertical component relative vorticity averaged over an area of $6^o \times 6^o$ on the ML center. Meso-α-scale lows generally form in the lower troposphere (e.g., below 700 hPa) in an environment of existing cyclonic vorticity. The maximum vorticity is most frequently located in the 850-700 hPa layer at the time of initial ML, but it is distributed almost evenly in the two layers of 700-500 hPa and 850-700 hPa at the time of ML over the Yellow Sea, when heavy rainfall may occur over the Korean Peninsula.

Structure of MLs, at or near the time of heavy rainfall over the Korean Peninsula, is described based on 1) vertical cross sections along the direction of vertical tilt of ML center and E-W vertical cross sections of height and temperature perturbations across an ML center at 850 hPa and 2) the horizontal distribution of height, temperature, winds, equivalent potential temperature and horizontal divergence at 925 hPa. Meso-α-scale lows show warm-core thermal structure in general. They are found to be tilted toward various directions with a majority of them (14 of 29 MLs) tilting northward with height.

Meso-α-scale lows near or at the time of heavy rainfall over the Korean Peninsula exhibit a common pattern of digging into the WPSH, which strengthens the height gradient and winds on their southeastern sides. As a result of these wind structures, high-θ_e air penetrates into these areas and near the ML center. Relatively strong convergence zones are present in the east of the ML centers where strong southwesterly meets a relatively weak easterly flow. These convergence zones can be favored sites of cloud cluster development. In addition, heavy rainfall can occur over the Korean Peninsula along these zones when the ML centers are still at a considerable distance from the Korean Peninsula.

The description of MLs in the present study is mainly based on NCEP CFSR data at 0.5^o spacing and 6-h time intervals. It is not clear how the current results depend on reanalysis and resolution. An increased resolution in a reanalysis can have effects on certain results (e.g., the location of initial ML occurrence, the horizontal structure of an ML, etc.).

Acknowledgments. This work was funded by the Korea Meteorological Administration Research and Development Program under Grant KMIPA 2015-5080. The authors wish to thank the anonymous reviewers for their valuable comments.

Edited by: Song-You Hong, Kim and Yeh

REFERENCES

Akiyama, T., 1978: Mesoscale pulsation of convective rain in medium-scale disturbances developed in Baiu front. *J. Meteor. Soc. Japan*, **56**, 267-283.

_____, 1984b: A medium-scale cloud cluster in a Baiu front. Part II: Thermal and kinematic fields and heat budgets. *J. Meteor. Soc. Japan*, **62**, 505-521.

Bao, X., and F. Zhang, 2013: Impacts of the mountain-plains solenoid and cold pool dynamics on the diurnal variation of warm-season precipitation over northern China. *Atmos. Chem. Phys.*, **13**, 6965-6982.

Bei, N. F., S. X. Zhao, and S. T. Gao, 2002: Numerical simulation of a heavy rainfall event in China during July 1998. *Meteor. Atmos. Phys.*, **80**, 153-164.

Chen, S.-J., and L. Dell'Osso, 1986: The effect of Qinghai-Tibet Plateau forcing on the meso-scale rain-bearing circulation systems over Eastern China during presummer rainy season. *J. Meteor. Soc. Japan*, **64**, 53-63.

_____, Y.-H. Kuo, P.-J. Zhang, and Q.-F. Bai, 1991: Synoptic climatology of cyclogenesis over East Asia, 1958-1987. *Mon. Wea. Rev.*, **119**, 1407-1418.

Ding, Y., Y. Zhang, M. Qiang, and H. Guoquan, 2001: Analyses of the large-scale circulation features and synoptic systems in East Asia during

the Intensive Observation Period of GAME/HUBEX. *J. Meteor. Soc. Japan*, **79**, 277-300.

Jung, W., and T.-Y. Lee, 2013: Formation and evolution of mesoscale convective systems that brought the heavy rainfall over Seoul on September 21, 2010. *Asia-Pac. J. Atmos. Sci.*, **49**, 635-647.

Lee, T.-Y., and Y.-H. Kim, 2007: Heavy precipitation systems over the Korean peninsula and their classification. *J. Korean Meteor. Soc*., **43**, 367-396.

Matsumoto, S., S. Yoshizumi, and M. Takeuchi, 1970: On the structure of the "Baiu Front" and the associated intermediate-scale disturbances in the lower atmosphere. *J. Meteor. Soc. Japan*, **48**, 479-491.

Murakami, T., and W.-G. Huang, 1984: Orographic effects of the Tibetan Plateau on the rainfall variations over central china during the 1979 summer. *J. Meteor. Soc. Japan*, **62**, 895-909.

Ninomiya, K., and T. Akiyama, 1971: The development of the medium-scale disturbance in the Baiu front. *J. Meteor. Soc. Japan*, **49**, 663-677.

_____, and K. Yamazaki, 1979: Heavy rainfalls associated with frontal depression in Asia subtropical humid region. Part 2. *J. Meteor. Soc. Japan*, **57**, 399-413.

_____, and H. Muraki, 1986: Large scale circulation over East Asia during Baiu period of 1979. *J. Meteor. Soc. Japan*, **64**, 409-429.

_____, and T. Akiyama, 1992: Multi-scale features of Baiu, the summer Monsoon over Japan and the east Asia. *J. Meteor. Soc. Japan*, **70**, 467-494.

Park, S.-U., I.-H. Yoon, and S.-K. Chung, 1986: Heat and moisture sources associated with the Changma front during the summer of 1978. *J. Korean Meteor. Soc*., **22**, 1-27.

Qian, J. H., W. K. Tao, and K. M. Lau, 2004: Mechanisms for torrential rain associated with the Mei-yu development during SCSMEX 1998. *Mon. Wea. Rev.*, **132**, 3-27.

Saha, S., and Coauthors, 2010: The NCEP Climate Forecast System Reanalysis. *Bull. Amer. Meteor. Soc.*, **91**, 1015-1057.

Shinoda, T., and H. Uyeda, 2002: Effective factors in the development of deep convective clouds over the wet region of eastern China during the summer monsoon season. *J. Meteor. Soc. Japan*, **80**, 1395-1414.

Tagami, H., H. Niino, and T. Kato, 2007: A study of meso-α-scale disturbances on the Baiu front and their environmental field. *J. Meteor. Soc. Japan*, **85**, 767-784.

Tochimoto, E., and T. Kawano, 2012: Development processes of Baiu frontal depressions. *Sci. Online Lett. Atmos.*, **8**, 9-12.

Wang, B., and I. Orlanski, 1987: Study of a heavy rain vortex formed over the eastern flank of the Tibetan Plateau. *Mon. Wea. Rev.*, **115**, 1370-1393.

Wang, C. C., and G. T. J. Chen, and R. E. Carbone, 2004: A climatology of warm-season cloud patterns over East Asia based on GMS infrared brightness temperature observations. *Mon. Wea. Rev.*, **132**, 1606-1609.

Yang, Y. M., W. L. Gu, R. L. Zhao, and J. Liu, 2010: The statistical analysis of low-level vortex during Mei-yu season in the lower reaches of the Yangtze (in Chinese). *J. Appl. Meteorol. Sci.*, **21**, 11-18.

Yoshizumi, S., 1977: On the structure of intermediate-scale disturbances on the Baiu front. *J. Meteor. Soc. Japan*, **55**, 107-120.

You, C.-H., D.-I. Lee, S.-M. Jang, M. Jang, H. Uyeda, T. Shinoda, and F. Kobayashi, 2010: Characteristics of rainfall systems accompanied with Changma front at Chujado in Korea. *Asia-Pac. J. Atmos. Sci.*, **46**, 41-51.

Zhang, Y., L. Zhang, C. Wang, Y. Xie, and Xiang, 2014: Mechanism of a torrential rainstorm that occurred to the west of a Mei-yu frontal low. *Asia-Pac. J. Atmos. Sci.*, **50**, 437-452.